Chemical Engineering Journal 316 (2017) 277–287

Contents lists available at ScienceDirect

Chemical Engineering Journal

journal homepage: www.elsevier.com/locate/cej

High-stable α-phase NiCo double hydroxide microspheres via microwave synthesis for supercapacitor electrode materials

Jing Li [a], Min Wei [a], Wei Chu [a,b,*], Ning Wang [c,*]

[a] Department of Chemical Engineering, Sichuan University, Chengdu 610065, People's Republic of China
[b] Key Laboratory of Green Chemistry and Technology of Ministry of Education (MOE), College of Chemistry, Sichuan University, Chengdu 610064, People's Republic of China
[c] Beijing Key Laboratory of Green Chemical Reaction Engineering and Technology, Department of Chemical Engineering, Tsinghua University, Beijing 100084, People's Republic of China

HIGHLIGHTS

- α-Phase NiCo double hydroxide (NiCo DH) was successfully synthesized via a rapid microwave heating method.
- The as-synthesized NiCo DH presented a 3D flower-like microsphere superstructure composed of ultrathin nanosheets.
- NiCo DH showed a long term stability at high current density.
- The asymmetric supercapacitor delivered a high energy density and good stability.

GRAPHICAL ABSTRACT

The 3D flower-like α-phase NiCo DH microsphere synthesized by microwave heating displayed excellent stability. The capacitance increased to 1220 F g^{-1} after 2000 cycles at 10 A g^{-1} (122.5% of its initial value of 996 F g^{-1}) and still remained a high capacitance of 822 F g^{-1} (93.8% retention) after another 1000 cycles at 30 A g^{-1}.

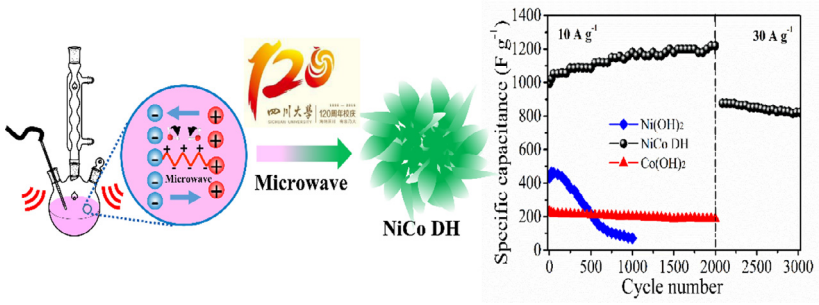

ARTICLE INFO

Article history:
Received 12 November 2016
Received in revised form 9 January 2017
Accepted 16 January 2017
Available online 17 January 2017

Keywords:
Supercapacitor
High stability
Microwave synthesis
NiCo double hydroxides
α-Phase
Microspheres

ABSTRACT

Fast and low-cost fabrication of high performance electrode materials is of great importance for the application of supercapacitors. Herein, in our research, three-dimensional (3D) flower-like NiCo double hydroxide (NiCo DH) microsphere was successfully synthesized via a rapid, inexpensive and energy-saving microwave route without using any template or surfactant under atmospheric pressure. The as-obtained NiCo DH microsphere endowed with α-phase structure with CNO^- ions intercalation in the interlayers (7.3 Å) was composed of ultrathin nanosheets with thickness less than 10 nm. Electrochemical test revealed the NiCo DH electrode showed a high specific capacitance of 1120 F g^{-1} at 1 A g^{-1} and remained 996 F g^{-1} at 10 A g^{-1} (88.9% retention). Moreover, after 2000 cycles, the capacitance reached 122.5% of its initial value at 10 A g^{-1} and still retained 93.8% at 30 A g^{-1} after another 1000 cycles, showing superb stability compared with reported α-phase hydroxides. The admirable stability could be attributed to the synergistic effect between Ni and Co elements, the ion exchange phenomenon between CNO^- and OH^- ions in the interlayer of NiCo DH during cycling test, and the coherent 3D superstructure. Besides, the asymmetric supercapacitor, with NiCo DH as positive electrode and activated carbon from coal as negative electrode, delivered a superior energy density of 42.5 Wh kg^{-1}. Consequently, the pleasant synthesis procedure and excellent integrated performance of NiCo DH enable it to be a promising electrode material for the energy storage devices.

* Corresponding authors at: Department of Chemical Engineering, Sichuan University, Chengdu 610065, People's Republic of China (W. Chu).
E-mail addresses: chuwei1965@scu.edu.cn (W. Chu), wangning860927@163.com (N. Wang).

http://dx.doi.org/10.1016/j.cej.2017.01.057
1385-8947/

1. Introduction

Supercapacitors have drawn great interest in recent years due to their fast charge and discharge rate, high power density, long cycle lifetime, and high reliability [1,2]. The energy is stored via either ion adsorption (electrochemical double layer capacitors, EDLCs) or fast surface redox reactions (pseudocapacitors) [3]. At present, the electrode materials have been the key of energy storage for supercapacitors. Carbon materials, such as activated carbon [4], carbon nanotubes [5], or graphene [6], and their hybrid materials [7], are typical electrode materials of EDLCs, usually possessing long cycle lifetime but poor capacitance [8]. Compared with EDLCs, pseudocapacitors, using metal oxides/hydroxides and conductive polymers as electrode materials, have better capacitance performance. Nevertheless, they suffer from either high cost and toxicity or unsatisfied cycle lifetime, which hindered their wide applications.

Recently, Ni based hydroxides and related metallic double hydroxides have drawn increasing interest as promising electrode materials. For example, partial substitution of Ni by some secondary metallic component could generally obtain Ni-M double hydroxides (M = Co [1], Mn [9], Al [10], or Ti [11]) with enhanced electrochemical performance. Among these, NiCo DH was the mostly investigated materials by virtue of its abundant feeding source, low toxicity, high theoretical capacitance and tunable composition [12–16]. Both NiCo DH and its counterpart exist in the form of two (α and β) kinds of phase. β-phase hydroxides are composed of brucite-like layers with an ordered close stack and a small interlayer spacing of 4.6 Å [17]. For α-phase, they consist of positively charged host layers and charge-balancing anions or molecules with a tunable interlayer spacing. As was reported before, Wang et al. synthesized three types of α-$Co(OH)_2$ with intercalated anions of dodecyl sulphate, benzoate and nitrate, which had a interlayer spacing of 1.6, 0.7 and 0.09 nm, respectively [18]. As a result, the sample with a larger interlayer spacing possessed the higher specific capacitance and better cycle life. This feature endowed α-phase hydroxides with higher specific capacitance than β-phase because more active sites in the interlayer can be gained during electrochemical reaction. While the weak interaction (Van der Waals force and hydrogen bonding) [19] between host layers and interlayer species makes α-phase hydroxides a sub-stable state and unsatisfied cycle life. So it remains a challenge for α-phase NiCo DH to both have the high capacitance and keep the good stability in basic solution.

Current synthesis of α-phase NiCo DH has been mainly confined to hydrothermal, chemical precipitation [9], or electrochemical deposition methods [20]. While these methods suffer from either harsh conditions or a long preparation duration and low yield. Of late, microwave synthesis of inorganic nanomaterials like transition metal oxides/hydroxides has drawn much attention owing to its advantages such as fast and uniform volume heating, accelerated nucleation and growth rate of nanomaterials [21–24], which have been used in electrocatalyst [25], supercapacitor [26], and lithium ion battery [27]. For example, Meher et al. synthesized NiO under microwave heating, exhibiting a higher capacitance than that by conventional-reflux [28]. Lei et al. have successfully fabricated 3D hierarchical $NiCo_2O_4$ microspheres that possess a high capacitance of 1006 F g^{-1} at 1 A g^{-1} and still retained 93.2% after 1000 cycles [29]. Inspired by this, we developed a green, facile and rapid microwave strategy to synthesize α-phase NiCo DH. We firstly explored the growth process of NiCo DH under microwave irradiation via a time-evolution experiment, and the synthesis duration was optimized. Then, the following work focused on the investigation of the electrochemical performance of NiCo DH. As a result, the as-synthesized α-phase NiCo DH microsphere showed a high specific capacitance, excellent rate capability, and especially, outstanding cycle life even at a large current density. The reasons for the better cycle life of NiCo DH were also explored. In addition, the asymmetric supercapacitor (ASC) using NiCo DH as positive electrode and activated carbon (AC) derived from coal as negative electrode showed a promising energy density and good stability.

2. Experimental section

2.1. Material synthesis

Typically, for the synthesis of NiCo DH sample, $NiCl_2{\cdot}6H_2O$ (1.5 mmol), $CoCl_2{\cdot}6H_2O$ (1.5 mmol), and urea (60 mmol) as precipitant were dissolved by deionized water (60 mL) in a 100 mL three-necked flask and stirred for 20 min to form transparent precursor solution. The resulting solution was placed in the microwave oven (XH-MC-1, Xianghu Co., Beijing) and heated under the microwave irradiation for various time (8–120 min) at 100 °C with the microwave power of 300 W (it took about 2 min to reach 100 °C from room temperature). After reaction, the mixture aged for 1 h and the resulting precipitation was collected and washed by deionized water thoroughly. The as-obtained product was dried in a vacuum at 60 °C for 24 h to get the NiCo DH powder.

The AC from coal was prepared based on our previous work [30]. In a typical procedure, the high ranked coal (3 g) was mixed with KOH at a KOH/coal ratio of 4, then the mixture was placed in a horizontal tubular furnace and activated at 800 °C for 2 h. After cooling down to room temperature, the sample was washed with 5 M HCl followed by distilled water to remove residual chemicals. Finally, the as-synthesized AC sample was dried at 110 °C overnight.

2.2. Characterization

The crystalline structure of NiCo DH samples was characterized by X-ray diffraction on a diffractometer (XRD, Haoyuan, DX-2700, China) using Cu Kα1 (λ = 1.5406 Å) radiation at 40 kV and 30 mA. The Fourier transform infrared (FT-IR) spectra were recorded with a FT-IR spectrometer (Bruker, Tensor, Germany) in the range of 400–4000 cm^{-1}. The specific surface area and pore structure of the materials were measured by N_2 adsorption/desorption using an automated surface area & pore size analyser (Quantachrome NOVA 1000e apparatus). The morphology and detailed structure of product were measured with a field emission scanning electron microscopy (FESEM, Hitachi, S3400, Japan) and a high-resolution transmission electron microscopy (HRTEM, JEOL, JEM-2010, Japan). The X-ray photoelectron spectra (XPS) were measured on a spectrometer (AXIS Ultra DLD) and corrected by the C 1s line at 284.6 eV.

2.3. Electrochemical tests

All the electrochemical tests of the as-obtained hydroxides and AC samples were conducted on a CHI 660E electrochemical workstation (Shanghai Chenhua Instrument Co., China) under a three-electrode configuration with a saturated Hg/HgO electrode as the reference electrode, a graphite sheet as the counter electrode in 6 M KOH aqueous solution. The working electrode was fabricated by mixing 80 wt.% NiCo DH powder, 10 wt.% acetylene black, and 10 wt.% poly (vinyldifluoride) in N-methylpyrrolidinone. The mixture was loaded on the Ni foam substrate (1 cm × 1 cm) and dried at 60 °C for 24 h. Then, the electrode was pressed under 10 MPa for 1 min. Generally, the mass loading of active material was around 3.2 mg.

The specific capacitance (SC) was calculated from the galvanostatic charge-discharge curves as follows:

$$Cs = I \times \Delta t/(\Delta V \times m) \quad (1)$$

where Cs, I, Δt, ΔV and m are the SC ($F\,g^{-1}$), the discharge current (A), the discharge time (s), the discharge potential range (V), and the mass of the active material (g), respectively. The electrochemical impedance spectroscopy (EIS) measurement was performed at open circuit potential with a frequency range from 0.01 kHz to 100 kHz, and an alternating current voltage of 5 mv amplitude.

The electrochemical performance of ASC device was tested under a two-electrode configuration with NiCo DH as positive electrode and AC as negative electrode in 6 M KOH electrolyte. To balance the charges stored on two electrodes, the mass loading ratio of active materials on two electrodes was calculated by following equation:

$$m_+/m_- = (C_- \times \Delta V_-)/(C_+ \times \Delta V_+) \quad (2)$$

where m, C, and ΔV are the mass of the active material, SC, and potential window of the electrode, respectively. "+" and "−" represent the positive and negative electrode, respectively. The SC value of ASC device was calculated from Eq. (1) based on the total mass loading of two electrodes. Here, the mass loading were 3.12 and 8.48 mg for NiCo DH and AC electrodes, respectively. The energy density and power density were calculated by equation as follow:

$$E = (C \times \Delta V^2)/7.2 \quad (3)$$

$$P = E \times 3600/t \quad (4)$$

where E ($Wh\,kg^{-1}$) and P ($W\,kg^{-1}$) are the energy density and power density, respectively.

3. Result discussion

3.1. Physicochemical characterization

The FT-IR spectra can reflect the functional groups of as-synthesized samples. As can be seen from Fig. 1, the narrow band at 3644 cm^{-1} ascribes to the O-H stretching vibration of non-hydrogen-bonded hydroxyl groups [31]. The band at 3441 cm^{-1} corresponds to the O-H stretching vibration of the hydrogen-bonded hydroxyl groups and the interlayer water molecules. The band at 1631 cm^{-1} belongs to the bending mode of the interlayer water molecules [32]. Peak around 640 cm^{-1} is due to the M-OH bending mode of Ni and Co, and the band below 500 cm^{-1} can be attributed to the M-O stretching vibration [33]. It is noteworthy that an intense band at about 2241 cm^{-1} can be observed, which is the typical stretching vibration of C≡N bonds in CNO^- anions, indicating the incomplete decomposition of urea [11,34]. According to the above information and other researchers' reports, the main reactions in the system can be deduced below [28,35].

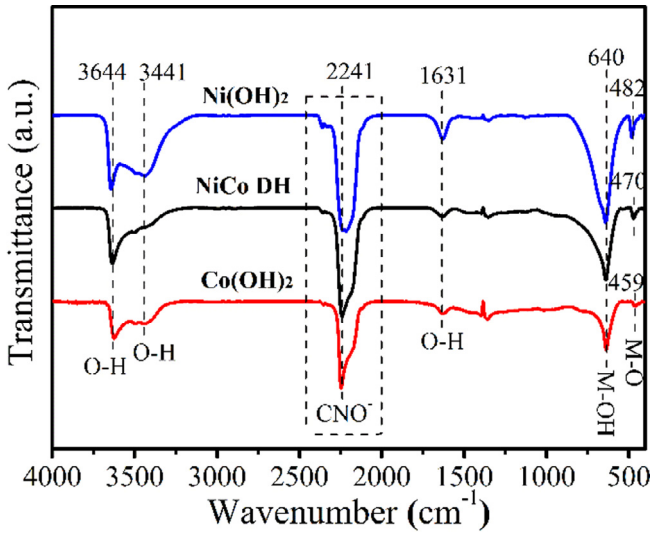

Fig. 1. FT-IR spectra of as-prepared samples for $Ni(OH)_2$, NiCo DH and $Co(OH)_2$.

$$NH_2CONH_2 \rightarrow NH_4^+ + CNO^-$$

$$CNO^- + 3H_2O \rightarrow HCO_3^- + NH_4^+ + OH^-$$

$$NH_2CONH_2 + H_2O \rightarrow 2NH_3 + CO_2$$

$$NH_3 + H_2O \rightarrow NH_4^+ + 2OH^-$$

The results of FT-IR provided the evidence for the formation of α-phase NiCo DH mainly intercalated with CNO^-, OH^-, and H_2O in the interlayer since there were not any interlayer ions in the β phase structure [35].

XRD was used to analyse the phase and crystallinity of the NiCo DH samples. The XRD patterns of NiCo DH prepared in various time are shown in Fig. 2a, where well-defined diffraction peaks located at 2θ value of 12.1, 24.5, 33.1, and 59.0° can be observed, which corresponds to the α-phase NiCo DH [32]. Interlayer spacing along the c-axis calculated by Bragg equation ($d = n\lambda/2\sin\theta$) from the (003) peak were all similar and equal to around 7.3 Å, which was relatively lower than generally reported LDHs (≈7.8 Å). The decrease of interlayer spacing resulted by the intercalation of CNO^- was due to the variation, arrangement and orientation of different intercalation anions [19,34]. Additionally, it was found that the intensity of (003) peak was gradually enhanced with the prolonged reaction time, while no obvious enhancement of other peaks was observed, suggesting a preferred orientation growth process of the crystal as reaction time went by [29]. The asymmetry of the (101) reflection demonstrated a random stack of the layers along the c-axis, leading to a formation of a turbostratic phase and the elimination of the (hkl) reflection [34]. In Fig. 2b, the peak intensity of NiCo DH became lower with respect to $Ni(OH)_2$, and the (110) peaks shifted to the low angle with the introduction of Co ions, leading to a change in d-spacing [12]. While the Co doping did not change the location of (003) peaks, with a interlayer spacing of 7.3 Å along the c-axis when assembling into the unit cell under microwave heating.

XPS measurement was conducted to determine the chemical composition and valence of NiCo DH. As presented in Fig. 3a, the main elements including Ni, Co, C, N, O were detected. For O 1s spectrum in Fig. 3b, the peak can be fitted by three parts at 530.5 eV, 531.3 eV and 532.4 eV that are assigned to M-O, M-OH, and absorbed water, respectively. In Ni 2p spectrum (Fig. 3c), two shakeup satellites (marked as "Sat.") close to two spin-orbit doublets at 873.4 eV (Ni $2p_{1/2}$) and 855.8 eV (Ni $2p_{3/2}$) with a spin-energy separation of 17.6 eV are the typical signals of Ni^{2+} [36]. In Co 2p spectrum (Fig. 3d), the two fitting peaks at 782.1 and 797.7 eV are attributed to Co^{2+}, while another fitting peaks at 780.4 and 796.4 eV are ascribed to Co^{3+}, suggesting the co-existence of Co^{2+} and Co^{3+} in NiCo DH [37]. It was reported that trivalent cations (such as Co^{3+}) substitution for Ni^{2+} could create a positive charge in the sheet, and the interlayer anions could compensate this extra charge, thus stabilizing the α-phase hydroxide, which would be beneficial to the electrochemical stability for NiCo DH [34,38]. The quantitative calculation of Ni/Co molar ratio on NiCo DH surface is approximately 1:1.1, which is consistent with its feeding ratio (1:1).

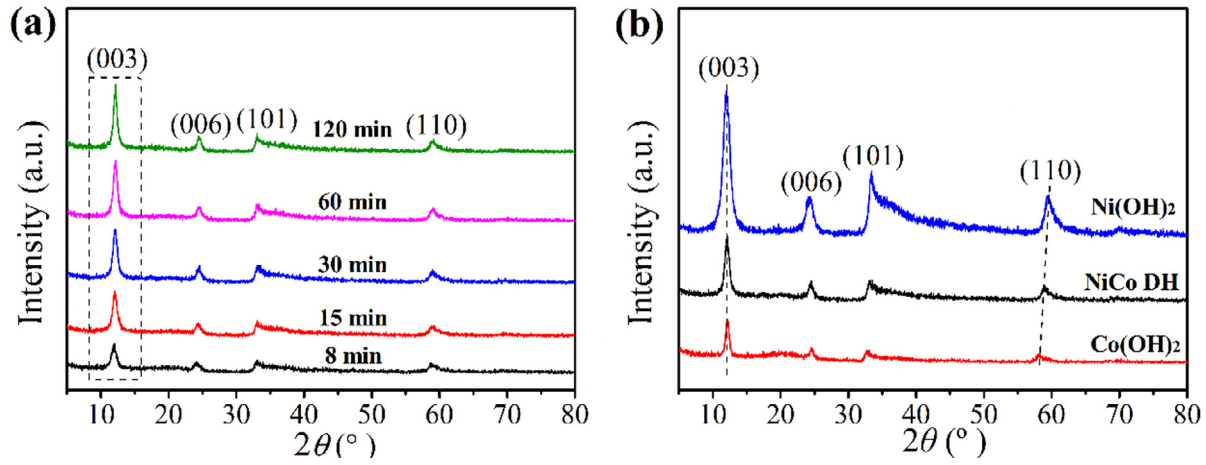

Fig. 2. XRD patterns of (a) NiCo DH collected at different microwave heating duration, (b) samples synthesized in 30 min for $Ni(OH)_2$, NiCo DH and $Co(OH)_2$.

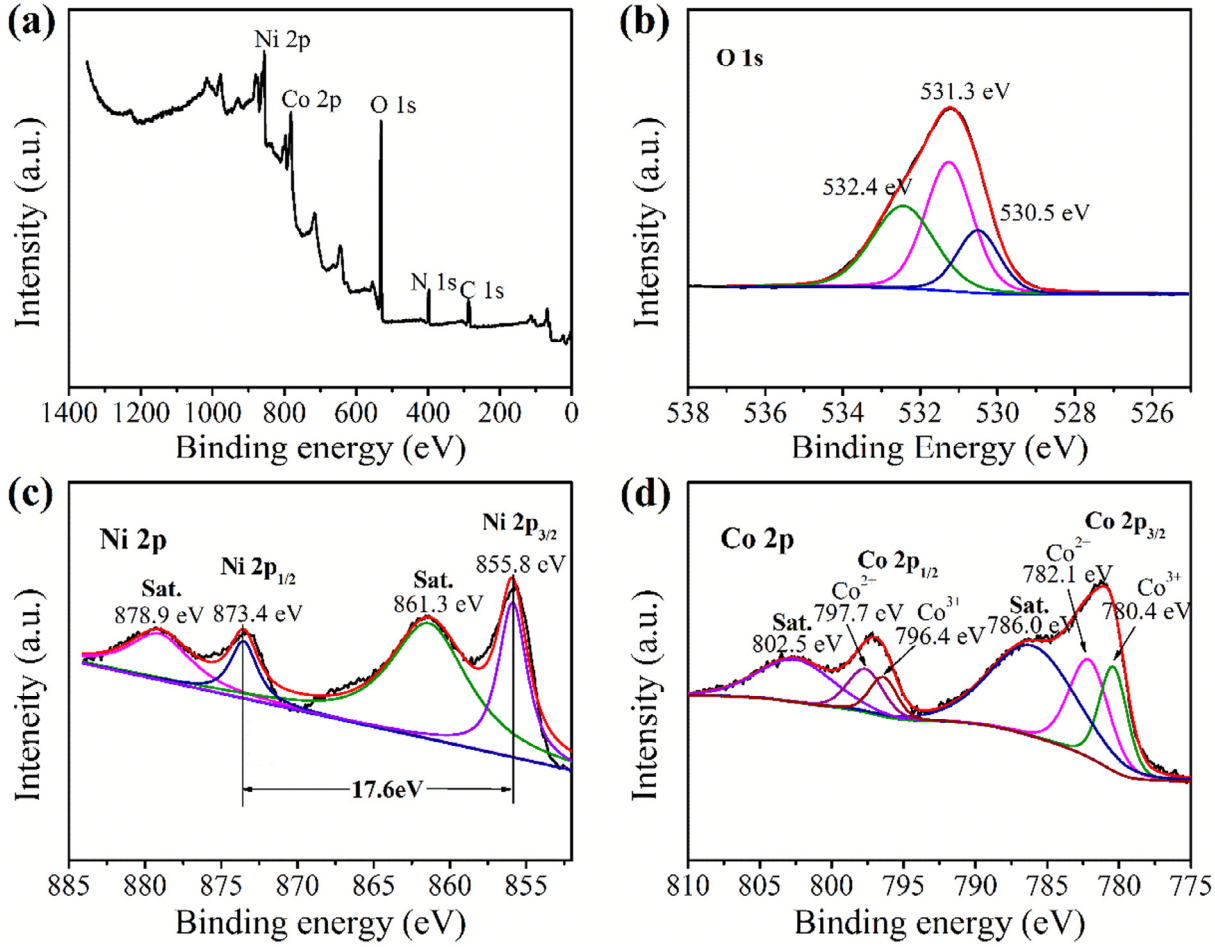

Fig. 3. XPS spectra of (a) survey spectrum, (b) O 1s, (c) Ni 2p, and (d) Co 2p for α-phase NiCo DH microsphere.

3.2. Proposed growth process of flower-like NiCo DH under microwave heating

The structure and morphology of NiCo DH was characterized by SEM, TEM and HRTEM. Fig. 4 and Fig. S1 showed the SEM images of NiCo DH synthesized at different reaction time under microwave heating. At 8 min (Fig. 4a and d), highly dispersed tiny submicrospheres can be observed. The average diameter of NiCo DH microsphere gradually increased with time and finally reached about 2.5 μm at 120 min (Fig. 4c and f). To have a clear insight of the detail structure of NiCo DH, TEM and HRTEM were conducted. The TEM image in Fig. 5a and b demonstrated the NiCo DH displayed the 3D flower-like superstructure and were composed of numerous petal-like nanosheets. The N_2 adsorption/desorption experiment revealed that this kind of 3D microspheres owned specific surface area of 9.2–26.4 $cm^2\ g^{-1}$, and presented a pore size

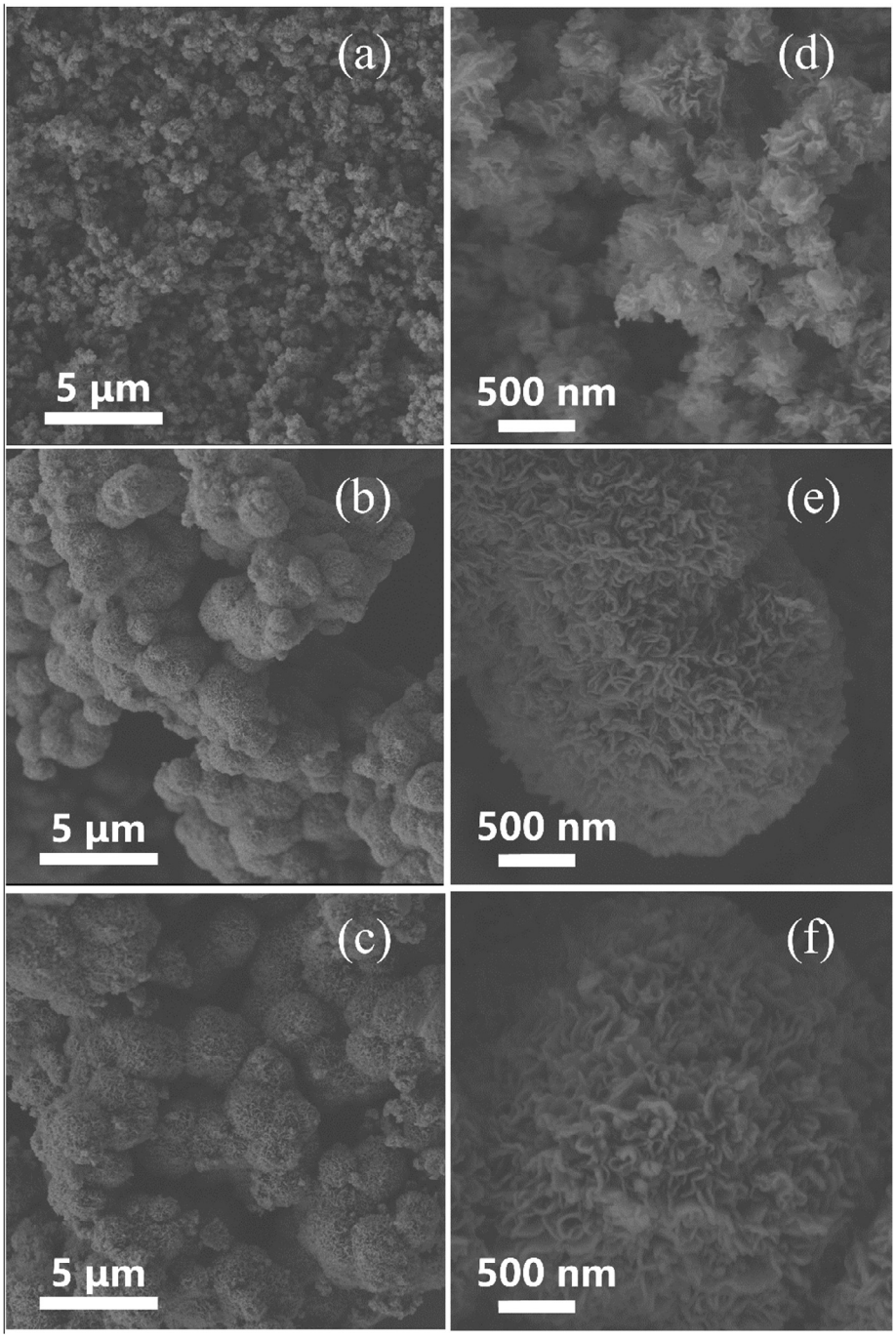

Fig. 4. SEM images of NiCo DH samples collected at different reaction time: (a, d) 8 min, (b, e) 30 min, (c, f) 120 min.

distribution in the range of 10–30 nm (Fig. S2). The thickness of the nanosheets from TEM image shown in Fig. 5b were measured to be less than 10 nm. The ultrathin feature may endowed NiCo DH with more accessible active sites and superior electrochemical performance. The detail structure of ultrathin nanosheet was further characterized by HRTEM. Fig. 5c showed flowerlike petal on the edge of the microsphere. In Fig. 5d, the HRTEM image along the c-axis of NiCo DH in vertical direction confirmed the (003) plane. The selected-area electron diffraction (SAED) patterns displayed three weak diffraction rings, corresponding to the (003), (101), (110) planes as identified by XRD.

The growth process of NiCo DH microsphere under microwave irradiation was proposed according to the above analysis and characterization (Fig. 6). It was reported that dipolar polarization and ionic conduction mechanisms involved in microwave heating contributed to the rapid synthesis of NiCo DH samples. As illustrated in Fig. 6a, polar molecules such as H_2O try to orientate with the rapidly changing alternating electric field, thus heat is generated by the rotation, friction, and collision of molecules. In the case of ions, Ni^{2+}, Co^{2+}, OH^-, Cl^-, CNO^- present in solution will move in the constantly changing directions through the solution based on the orientation of the electric field, causing a local temperature rise due to friction and collision [24]. In this procedure, the assembly of positively charged host layers, and interlayer ions/molecules into NiCo DH unit cell (Fig. 6b) was accelerated in the presence of electric field, and this assembly process may involve the electrostatic interaction, Van der Waals force and hydrogen-bond interaction [39].

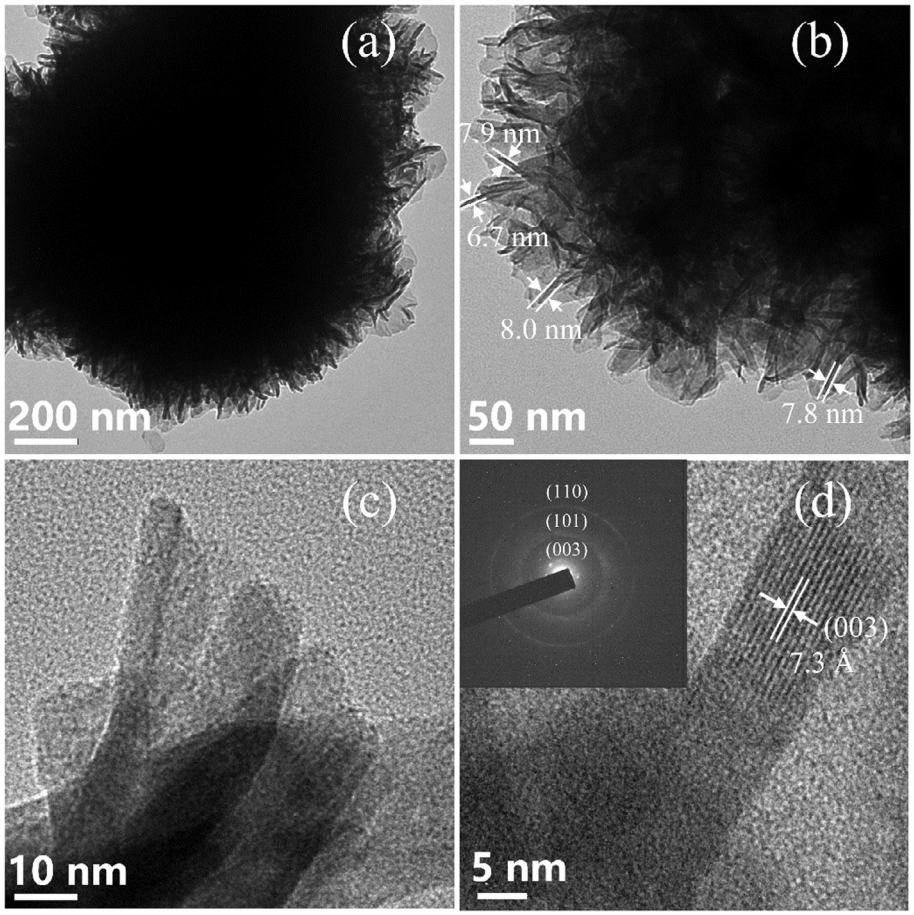

Fig. 5. TEM (a, b) and HRTEM (c, d) images of NiCo DH (inset: SAED patterns) synthesized in 30 min.

It should be pointed out that at the first reaction duration of 4 min, we did not collected the precipitate, indicating the concentration of the precursor monomer solution had not reached the point of equilibrium concentration when the nucleation began. When the "burst nucleation" point was reached around 8 min, the number of primary nuclei (Fig. 6c) increased sharply accompanied by the gradual reduction of the monomers concentration [40]. As the initially formed tiny crystals were thermodynamically unstable, they aggregated together to minimize the interfacial energy and formed the aggregated sub-microsphere as revelled in Fig. 6d. And then, the precursor reactant orientedly attached to the specific plane, forming the ultrathin nanosheets (Fig. 6e and f). This oriented attachment growth process was in good accordance with the XRD result (Fig. 2a). The further oriented growth and self-assemble with

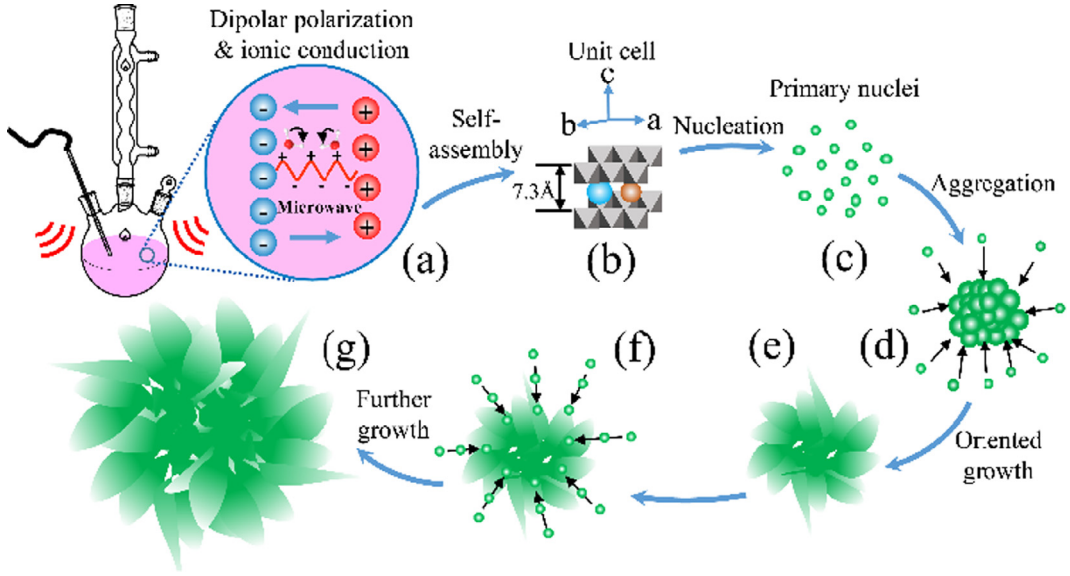

Fig. 6. Proposed growth process of NiCo DH microsphere under microwave irradiation.

the increased time led to the formation of final 3D flower-like NiCo DH microsphere (Fig. 6g).

3.3. Electrochemical performance

The SC of NiCo DH samples synthesized at different time was calculated from CD curves shown in Fig. 7a. The results revelled that the sample owned the SC of 1314, 1120, 1044 F g^{-1} at the different reaction time of 8, 30 and 120 min, respectively. It was believed that the accessible active surface area of electrode materials exposed in electrolyte played an important role in the capacitance performance [41]. So the highest SC of NiCo DH prepared in 8 min can be attributed to the high dispersion and the less aggregation of the NiCo DH microsphere. Fig. 7b showed the EIS results. The semicircle in high frequency region is an indicative of charge transfer resistance (R_{ct}) and the slope of the Warburg impedance plot in low frequency region is related to the ion or electrolyte diffusion resistance [42]. The R_{ct} of NiCo DH synthesized in 8 min was estimated to be 0.48 Ω, which was lower than that in 30 min (0.50 Ω) and 120 min (0.65 Ω), suggesting the smallest charge transfer resistance caused by Faradaic reaction. Due to the continuous assembly and growth, the NiCo DH superstructure showed the largest diameter up to about 2.5 μm (Fig. 5c) at 120 min, which could obviously lengthen the diffusion pass of electrolyte ions, thus the Warburg impedance was the highest compared with the sample synthesized in shorter duration. The above results indicated that the overgrowth of the NiCo DH microsphere may result in the dead volume that could not be utilized efficiently, thus reducing the accessible active surface area and increasing the diffusion pass of electrolyte ions. Therefore, we optimized the reaction time at 30 min considering the product yield and performance of NiCo DH.

The electrochemical properties of NiCo DH and its unitary hydroxides were firstly investigated by cyclic voltammetry (CV) (Fig. S3). Fig. 8a shows typical CV curves at a scan rate of 10 mV s^{-1}. The average areas of CV curves indicated the as-obtained NiCo DH possessed a significant higher specific capacitance than $Ni(OH)_2$ or $Co(OH)_2$. The well-defined redox peaks within 0.0–0.6 V indicated the nature of the Faradaic reaction of the active phase on the interface of the electrode materials by the following equations:

$$Ni(OH)_2 + OH^- \leftrightarrow NiOOH + H_2O + e^- \quad (5)$$

$$Co(OH)_2 + OH^- \leftrightarrow CoOOH + H_2O + e^- \quad (6)$$

$$CoOOH + OH^- \leftrightarrow CoO_2 + H_2O + e^- \quad (7)$$

The galvanostatic charge-discharge (GCD) curves of NiCo DH samples at different current densities are shown in Fig. 8b, the platform revealed in the discharge curves demonstrated the typical pseudocapacitor behaviour of NiCo DH. To evaluate the rate capability, specific capacitance was tested in the current density from 1 to 20 A g^{-1}. As can be seen from Fig. 8c, NiCo DH possessed a high specific capacitance of 1120 F g^{-1} at 1 A g^{-1}, and 1117, 1075, 996, 948 F g^{-1} at 2, 5, 10, 15 A g^{-1}, and even remained 892 F g^{-1} at 20 A g^{-1} (79.6% retention), showing excellent rate capability compared to the unitary nickel hydroxide or cobalt hydroxide, which only retained 40.0% and 62.4% when current density increased from 1 to 20 A g^{-1}, respectively. The enhanced rate capability was attributed to the following reasons. Firstly, recent work investigated by the density functional theory has demonstrated that Co doping can effectively reduce the band gap to increase the conductivity of NiCo DH because a smaller band gap means a larger probability for electrons jumping from the valence band to the conduction band [43]. Secondly, the more conductive CoOOH species formed in the electrochemical oxidation of $Co(OH)_2$ as described in the Eq. (6) [15,44,45].

Cycling stability is another important performance index for supercapacitor in practical application. As α-phase hydroxide is usually metastable and quickly transforms into β phase in strong alkali solution, resulting in a rapid decline in specific capacitance, thus α hydroxides owning high specific capacitance and excellent stability in strong alkali are desired. The cycling tests results are shown in Fig. 8d, and the as-obtained samples were firstly tested by continuous charge-discharge at a current density of 10 A g^{-1}. Surprisingly, the specific capacitance of NiCo DH did not decline but increased to 122.5% of the initial SC after 2000 cycling test (from 996 to 1220 F g^{-1}), while $Co(OH)_2$ remained 81.7% after 2000 cycles and $Ni(OH)_2$ only remained 16.7% after 1000 cycles. What's more, another 1000 CD cycles of NiCo DH conducted at 30 A g^{-1} revealed that the capacitance could still remain 93.8% at such a large current density, displaying superb stability compared to some previous reports (Table S1) [46–57].

3.4. Reasons for the high stability of NiCo DH

The reasons for the increase of specific capacitance for NiCo DH after cycle test compared with $Ni(OH)_2$ and $Co(OH)_2$ were explored.

Firstly, an important factor of maintaining the good stability was due to the Co doping because the introduction of Co^{3+} could compensate the interlayer anions, which could stabilize the

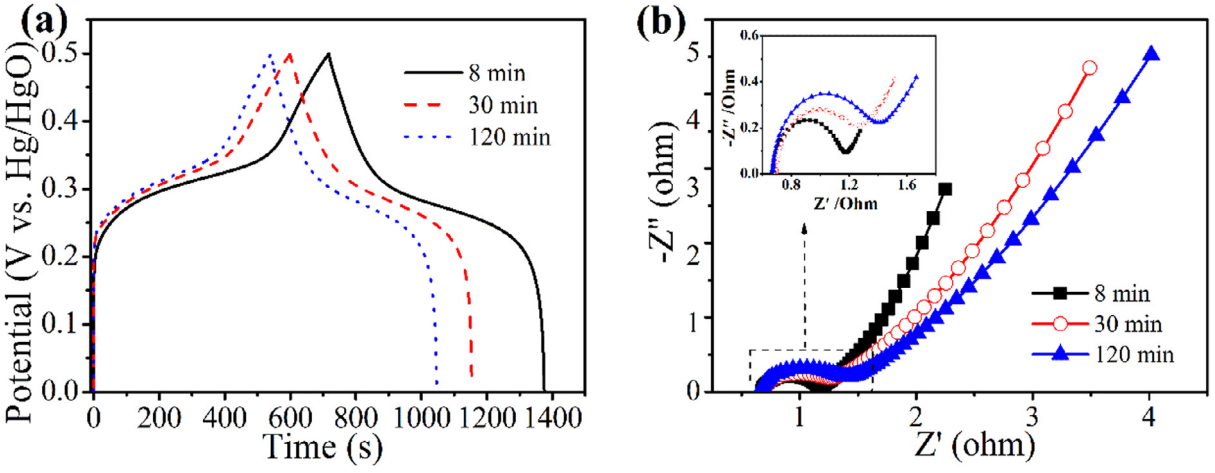

Fig. 7. (a) CD curves, (b) EIS spectra of NiCo DH samples collected at different reaction time (inset: enlarged high frequency region of Nyquist plot).

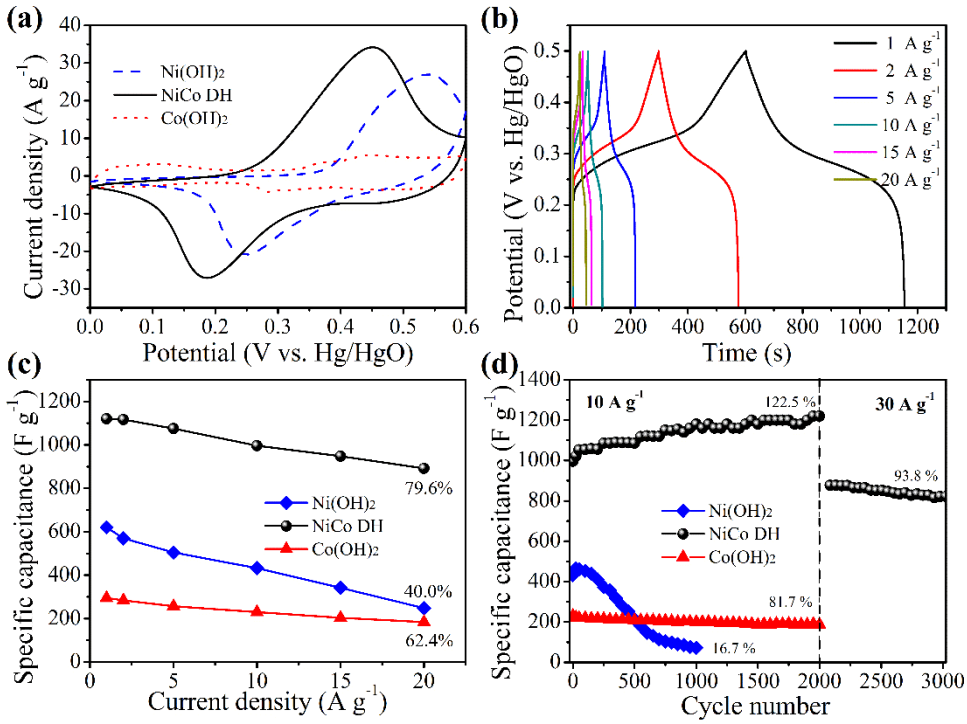

Fig. 8. (a) Comparison of CV curves of NiCo DH with its unitary hydroxides at a scan rate of 10 mV s^{-1}, (b) CD curves of NiCo DH at various current densities, specific capacitance (c) and cycling stability (d) of NiCo DH and its unitary hydroxides.

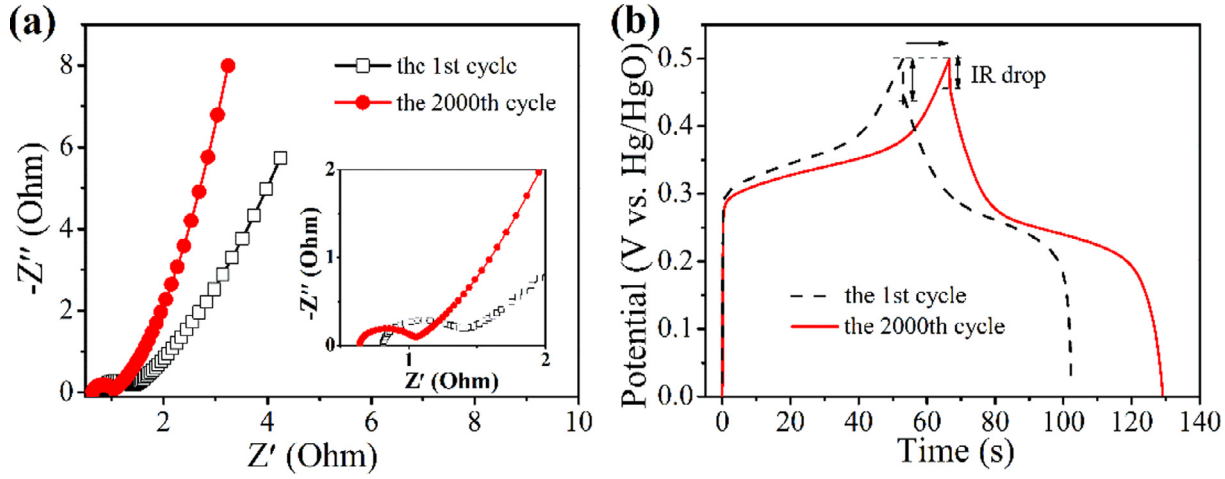

Fig. 9. EIS spectra (inset: enlarged high frequency region of Nyquist plot) (a), and CD curves (b) of NiCo DH at the first and the 2000th cycling test at 10 A g^{-1}.

α-phase hydroxides as analysed in previous XPS result. As indicated by TEM in Fig. S4, the morphology of NiCo DH after cycling remained nearly unchanged. While for $Ni(OH)_2$ and $Co(OH)_2$, the nanosheets on the microsphere exfoliated or destroyed. Therefore, the synergistic effect between Ni and Co make sure that NiCo DH can keep a more stable state than unitary $Ni(OH)_2$ or $Co(OH)_2$ in KOH electrolyte.

Secondly, the coherent superstructure of NiCo DH microsphere could not be fully wetted and accessed by OH^- at the first several CD cycles, and the further permeation of electrolyte ions to the electrode surface in the inner region led to the capacitance promotion. This increase trend can be also observed for close-connected $Ni(OH)_2$ microspheres shown in Fig. S5d at initial CD cycles (Fig. 8d). While for $Co(OH)_2$ with open structure, ion transport become easier as identified by EIS results (Fig. S5), which may result to the disappearance of initial activation.

Thirdly, in an attempt to better understand the capacitance promotion stage of NiCo DH in cycling of this work, the impedance measurement was conducted before and after cycling. As can be seen from Fig. 9a, the width of semicircle in the high frequency region became smaller after cycling, which indicated the more rapid electron transfer to the electrode material. In the low frequency region, the slope of impedance plot is larger than that before the cycling test, suggesting a more rapid ions diffusion rate to the interface of the electrode material. The smaller IR drop after cycling from CD result also demonstrated it (Fig. 9b). Subsequently,

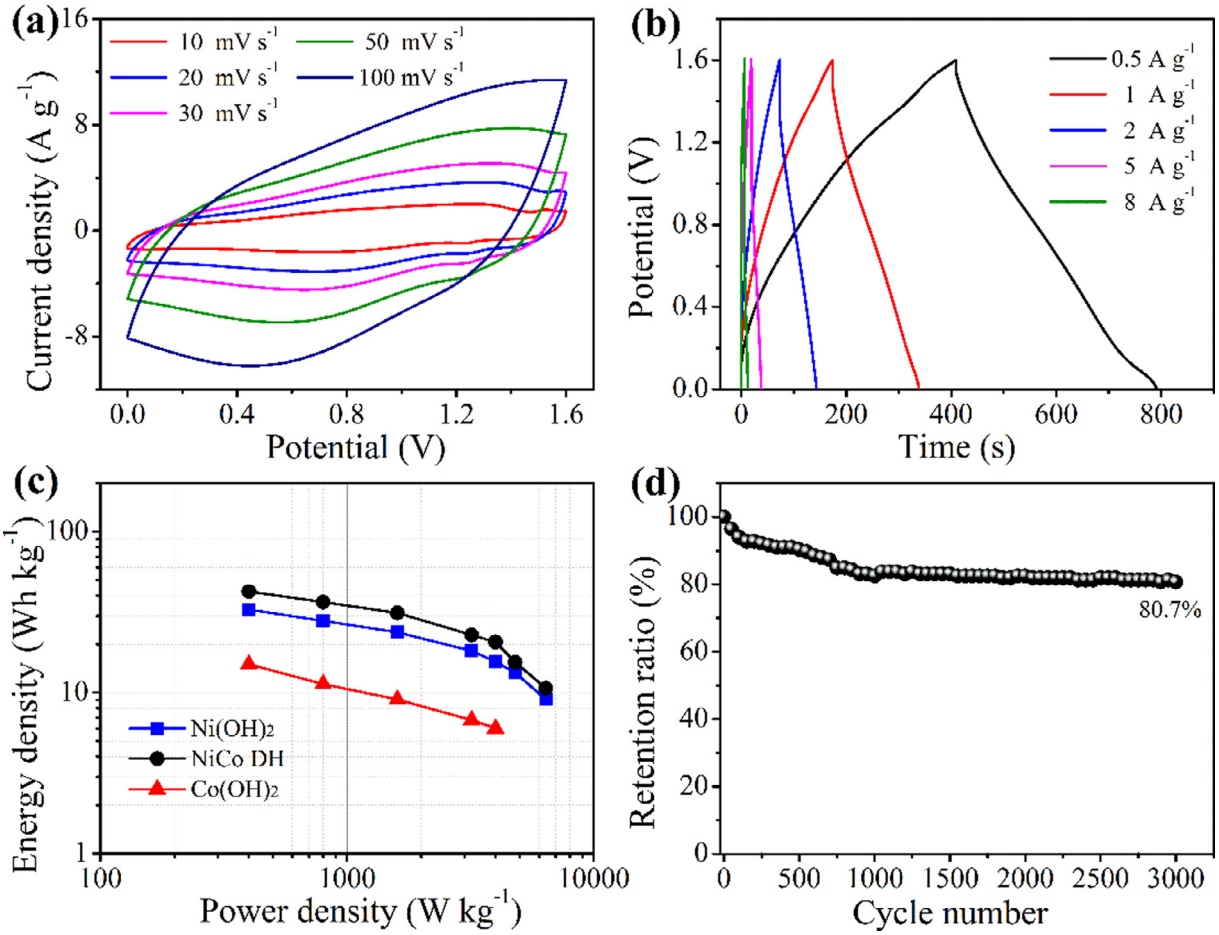

Fig. 10. (a) CV curves of the NiCo DH//AC ASC at different scan rates, (b) CD curves of the NiCo DH//AC ASC at different current densities, (c) Ragone plot of NiCo DH and its unitary hydroxides, (d) cycling performance of NiCo DH//AC ASC at a current density of 5 A g^{-1}.

XRD was carried out to identify the component and phase transformation after 2000 CD cycles displayed in Fig. S6. It was found that the (003) peak shifted a little bit to the low angle which corresponded to the α-phase hydroxides intercalated with OH^-, and the interlayer spacing changed from 7.3 Å to 7.8 Å, accordingly. The XRD result revealed that ion exchange between CNO^- and OH^- happened in the interlayer of NiCo DH during electrochemical test in 6 M KOH. In this case, continually substitution of CNO^- by OH^- allowed more active redox sites gradually exposed in the electrolyte directly, thus leading to the increase of specific capacitance during the test. In addition, the interlayer could act as an "ion-buffering reservoir", shortening the diffusion distance of OH^- to the active sites on the host layers [58], which contributed to the rapid ion transfer as analysed by EIS result. For example, Wang et al. reported that α-$Co(OH)_2$ with a larger interlayer spacing showed much better rate capability and stability [18]. Furthermore, the comparative sample with a interlayer spacing of 7.8 Å synthesized using NH_4OH as precipitant also showed much more rapid electrolyte diffusion rate from EIS result shown in Fig. S7, further demonstrating OH^- intercalated in the interlayer helped to the rapid ion diffusion.

3.5. Electrochemical performance of ASC

An asymmetric supercapacitor with AC from coal as negative electrode was fabricated to illustrate the potential application of the NiCo DH electrode. Fig. S8a shows the CV curves of AC electrode at different scan rates from 10 to 100 mV s^{-1}. The CV curves remain the regular rectangular shape, indicating the typical electric double-layer capacitance property of AC. The CD curves and the capacitance values at different current density are also shown in Fig. S8b and c. Owing to the high specific surface area and narrow pore size distribution as well as good conductivity [30], the AC electrode exhibited high SC of 176 F g^{-1} at 1 A g^{-1} and 124 F g^{-1} at 10 A g^{-1}. The CV and CD curves of ASCs are shown in Fig. 10a and b, the SC based on the total mass was calculated to be 119.5 F g^{-1} at 1 A g^{-1}. From the Ragone plot shown in Fig. 10c, NiCo DH displayed the higher energy density than monometallic $Ni(OH)_2$ and $Co(OH)_2$, and delivered a high energy density of 42.5 Wh kg^{-1} at a power density of 400 W kg^{-1}, which was comparable to many other reports [13,46,48,53,59–63]. (Table S2). More detailed performance parameters were shown in Table S3. In addition, the cycling life of as-fabricated ASC was also evaluated. As indicated in Fig. 10d, the capacitance retention rate is 80.7% of its initial capacitance after 3000 cycles, showing good stability. The comprehensive performance reveals that the NiCo DH is a promising electrode material as the candidate for the energy storage system.

4. Conclusions

In summary, we have successfully fabricated the 3D flower-like NiCo DH microsphere superstructure via a simple, rapid and low-price microwave assisted route. The microsphere composed of ultrathin nanosheets followed the oriented attachment growth process under microwave heating. The as-synthesized α-phase

NiCo DH exhibited a high specific capacitance (1120 F g^{-1} at 1 A g^{-1}), excellent rate capability (88.9% retention at 10 A g^{-1}), and remarkable stability (122.5% of its initial value at 10 A g^{-1} after 2000 cycles and 93.8% retention at 30 A g^{-1} after another 1000 cycles). The synergistic effect between Ni and Co dramatically enhanced the stability of NiCo DH compared with unitary Ni $(OH)_2$ or $Co(OH)_2$. The coherent superstructure of NiCo DH and the ion-exchange phenomenon contributed to the increase of specific capacitance in KOH. Additionally, the as-fabricated ASC delivered a high energy density and good stability.

Acknowledgements

This work was supported by the National Natural Science Foundation of China (No. 21476145). We thank Dr. Y.P. Zhou, Y.C. Zhu, Z. Peng, W.Su, and Dr. J. Deng for their useful discussion and helps.

Appendix A. Supplementary data

Supplementary data associated with this article can be found, in the online version, at http://dx.doi.org/10.1016/j.cej.2017.01.057.

References

[1] H. Chen, L. Hu, M. Chen, Y. Yan, L. Wu, Nickel-cobalt layered double hydroxide nanosheets for high-performance supercapacitor electrode materials, Adv. Funct. Mater. 24 (2014) 934–942.
[2] J.T. Zhang, J.W. Jiang, H.L. Li, X.S. Zhao, A high-performance asymmetric supercapacitor fabricated with graphene-based electrodes, Energy Environ. Sci. 4 (2011) 4009–4015.
[3] P. Simon, Y. Gogotsi, Materials for electrochemical capacitors, Nat. Mater. 7 (2008) 845–854.
[4] B. Li, F. Dai, Q. Xiao, L. Yang, J. Shen, C. Zhang, M. Cai, Nitrogen-doped activated carbon for a high energy hybrid supercapacitor, Energy Environ. Sci. 9 (2016) 102–106.
[5] L.L. Zhang, X.S. Zhao, Carbon-based materials as supercapacitor electrodes, Chem. Soc. Rev. 38 (2009) 2520–2531.
[6] X. Cao, Y. Shi, W. Shi, G. Lu, X. Huang, Q. Yan, Q. Zhang, H. Zhang, Preparation of novel 3D graphene networks for supercapacitor applications, Small 7 (2011) 3163–3168.
[7] Z. Fan, J. Yan, L. Zhi, Q. Zhang, T. Wei, J. Feng, M. Zhang, W. Qian, F. Wei, A three-dimensional carbon nanotube/graphene sandwich and its application as electrode in supercapacitors, Adv. Mater. 22 (2010) 3723–3728.
[8] G. Wang, L. Zhang, J. Zhang, A review of electrode materials for electrochemical supercapacitors, Chem. Soc. Rev. 41 (2012) 797–828.
[9] J.W. Zhao, J. Chen, S.M. Xu, M.F. Shao, Q. Zhang, F. Wei, J. Ma, M. Wei, D.G. Evans, X. Duan, Hierarchical NiMn layered double hydroxide/carbon nanotubes architecture with superb energy density for flexible supercapacitors, Adv. Funct. Mater. 24 (2014) 2938–2946.
[10] J.C. Huang, T. Lei, X.P. Wei, X.W. Liu, T. Liu, D.X. Cao, J.L. Yin, G.L. Wang, Effect of Al-doped beta-$Ni(OH)_2$ nanosheets on electrochemical behaviors for high performance supercapacitor application, J. Power Sources 232 (2013) 370–375.
[11] Y.F. Zhao, Q. Wang, T. Bian, H.J. Yu, H. Fan, C. Zhou, L.Z. Wu, C.H. Tung, D. O'Hare, T.R. Zhang, Ni^{3+} doped monolayer layered double hydroxide nanosheets as efficient electrodes for supercapacitors, Nanoscale 7 (2015) 7168–7173.
[12] G. Chen, S.S. Liaw, B. Li, Y. Xu, M. Dunwell, S. Deng, H. Fan, H. Luo, Microwave-assisted synthesis of hybrid $Co_xNi_{1-x}(OH)_2$ nanosheets: tuning the composition for high performance supercapacitor, J. Power Sources 251 (2014) 338–343.
[13] M. Jing, H. Hou, C.E. Banks, Y. Yang, Y. Zhang, X. Ji, Alternating voltage introduced NiCo double hydroxide layered nanoflakes for an asymmetric supercapacitor, ACS Appl. Mater. Interfaces 7 (2015) 22741–22744.
[14] X. Sun, G.K. Wang, H.T. Sun, F.Y. Lu, M.P. Yu, J. Lian, Morphology controlled high performance supercapacitor behaviour of the Ni-Co binary hydroxide system, J. Power Sources 238 (2013) 150–156.
[15] H.C. Chen, J.J. Jiang, L. Zhang, Y.D. Zhao, D.Q. Guo, Y.J. Ruan, D.D. Xia, One-pot fabrication of layered alpha-phase nickel-cobalt hydroxides as advanced electrode materials for pseudocapacitors, Chempluschem 80 (2015) 181–187.
[16] W. Quan, Z.L. Tang, Y. Hong, S.T. Wang, Z.T. Zhang, Hydroxyl compensation effects on the cycle stability of Nickel-Cobalt layered double hydroxides synthesized via solvothermal method, Electrochim. Acta 182 (2015) 445–451.
[17] R.Z. Ma, J.B. Liang, X.H. Liu, T. Sasaki, General insights into structural evolution of layered double hydroxide: underlying aspects in topochemical transformation from brucite to layered double hydroxide, J. Am. Chem. Soc. 134 (2012) 19915–19921.
[18] L. Wang, Z.H. Dong, Z.G. Wang, F.X. Zhang, J. Jin, Layered-$Co(OH)_2$ nanocones as electrode materials for pseudocapacitors: understanding the effect of interlayer space on electrochemical activity, Adv. Funct. Mater. 23 (2013) 2758–2764.
[19] D.G. Evans, R.C.T. Slade, Structural aspects of layered double hydroxides, in: X. Duan, D.G. Evans (Eds.), Layered Double Hydroxides, 2006, pp. 1–87.
[20] X.C. Li, J.J. Shen, W. Sun, X.D. Hong, R.T. Wang, X.H. Zhao, X.B. Yan, A super-high energy density asymmetric supercapacitor based on 3D core-shell structured NiCo-layered double hydroxide@carbon nanotube and activated polyaniline-derived carbon electrodes with commercial level mass loading, J. Mater. Chem. A 3 (2015) 13244–13253.
[21] S. Faraji, F.N. Ani, Microwave-assisted synthesis of metal oxide/hydroxide composite electrodes for high power supercapacitors – a review, J. Power Sources 263 (2014) 338–360.
[22] I. Bilecka, M. Niederberger, Microwave chemistry for inorganic nanomaterials synthesis, Nanoscale 2 (2010) 1358–1374.
[23] M. Tsuji, M. Hashimoto, Y. Nishizawa, M. Kubokawa, T. Tsuji, Microwave-assisted synthesis of metallic nanostructures in solution, Chem. Eur. J. 11 (2005) 440–452.
[24] Y.J. Zhu, F. Chen, Microwave-assisted preparation of inorganic nanostructures in liquid phase, Chem. Rev. 114 (2014) 6462–6555.
[25] C. Qiao, Y. Zhang, Y.Q. Zhu, C.B. Cao, X.H. Bao, J.Q. Xu, One-step synthesis of zinc-cobalt layered double hydroxide (Zn-Co-LDH) nanosheets for high-efficiency oxygen evolution reaction, J. Mater. Chem. A 3 (2015) 6878–6883.
[26] Y.Q. Zhu, C.B. Cao, S. Tao, W.S. Chu, Z.Y. Wu, Y.D. Li, Ultrathin nickel hydroxide and oxide nanosheets: synthesis, characterizations and excellent supercapacitor performances, Sci. Rep. 4 (2014) 5787.
[27] Y.Q. Zhu, C.B. Cao, J.T. Zhang, X.Y. Xu, Two-dimensional ultrathin $ZnCo_2O_4$ nanosheets: general formation and lithium storage application, J. Mater. Chem. A 3 (2015) 9556–9564.
[28] S.K. Meher, P. Justin, G.R. Rao, Microwave-mediated synthesis for improved morphology and pseudocapacitance performance of nickel oxide, ACS Appl. Mater. Interfaces 3 (2011) 2063–2073.
[29] Y. Lei, J. Li, Y.Y. Wang, L. Gu, Y.F. Chang, H.Y. Yuan, D. Xiao, Rapid microwave-assisted green synthesis of 3D hierarchical flower-shaped $NiCo_2O_4$ microsphere for high-performance supercapacitor, ACS Appl. Mater. Interfaces 6 (2014) 1773–1780.
[30] Z. Peng, Z.L. Guo, W. Chu, M. Wei, Facile synthesis of high-surface-area activated carbon from coal for supercapacitors and high CO_2 sorption, RSC Adv. 6 (2016) 42019–42028.
[31] S. Vijayakumar, S. Nagamuthu, G. Muralidharan, Supercapacitor studies on NiO nanoflakes synthesized through a microwave route, ACS Appl. Mater. Interfaces 5 (2013) 2188–2196.
[32] J. Yan, Z.J. Fan, W. Sun, G.Q. Ning, T. Wei, Q. Zhang, R.F. Zhang, L.J. Zhi, F. Wei, Advanced asymmetric supercapacitors based on $Ni(OH)_2$/graphene and porous graphene electrodes with high energy density, Adv. Funct. Mater. 22 (2012) 2632–2641.
[33] M. Li, K.Y. Ma, J.P. Cheng, D.H. Lv, X.B. Zhang, Nickel-cobalt hydroxide nanoflakes conformal coating on carbon nanotubes as a supercapacitive material with high-rate capability, J. Power Sources 286 (2015) 438–444.
[34] B. Mavis, M. Akinc, Cyanate intercalation in nickel hydroxide, Chem. Mater. 18 (2006) 5317–5325.
[35] L.P. Xu, Y.S. Ding, C.H. Chen, L.L. Zhao, C. Rimkus, R. Joesten, S.L. Suib, 3D flowerlike alpha-nickel hydroxide with enhanced electrochemical activity synthesized by microwave-assisted hydrothermal method, Chem. Mater. 20 (2008) 308–316.
[36] J.B. Liang, R.Z. Ma, N.B.O. Iyi, Y. Ebina, K. Takada, T. Sasaki, Topochemical synthesis, anion exchange, and exfoliation of Co-Ni layered double hydroxides: a route to positively charged Co-Ni hydroxide nanosheets with tunable composition, Chem. Mater. 22 (2010) 371–378.
[37] J. Jiang, A.L. Zhang, L.L. Li, L.H. Ai, Nickel-cobalt layered double hydroxide nanosheets as high-performance electrocatalyst for oxygen evolution reaction, J. Power Sources 278 (2015) 445–451.
[38] C. Faure, C. Delmas, M. Fouassier, P. Willmann, Preparation and characterization of cobalt-substituted alpha-nickel hydroxides stable in KOH medium part 1. α′-hydroxide with an ordered packing, J. Power Sources 35 (1991) 249–261.
[39] Y.Q. Zhu, H.Z. Guo, H.Z. Zhai, C.B. Cao, Microwave-assisted and gram-scale synthesis of ultrathin SnO_2 nanosheets with enhanced lithium storage properties, ACS Appl. Mater. Interfaces 7 (2015) 2745–2753.
[40] Z.H. Wu, S.L. Yang, W. Wu, Shape control of inorganic nanoparticles from solution, Nanoscale 8 (2016) 1237–1259.
[41] K. Fan, H. Chen, Y.F. Ji, H. Huang, P.M. Claesson, Q. Daniel, B. Philippe, H. Rensmo, F.S. Li, Y. Luo, L.C. Sun, Nickel-vanadium monolayer double hydroxide for efficient electrochemical water oxidation, Nat. Commun. 7 (2016) 11981.
[42] S. Khalid, C.B. Cao, L. Wang, Y.Q. Zhu, Microwave assisted synthesis of porous $NiCo_2O_4$ microspheres: application as high performance asymmetric and symmetric supercapacitors with large areal capacitance, Sci. Rep. 6 (2016) 22699.
[43] J. Wu, W.W. Liu, Y.X. Wu, T.C. Wei, D.S. Geng, J. Mei, H. Liu, W.M. Lau, L.M. Liu, Three-dimensional hierarchical interwoven nitrogen-doped carbon nanotubes/Co_xNi_{1-x}-layered double hydroxides ultrathin nanosheets for high-performance supercapacitors, Electrochim. Acta 203 (2016) 21–29.
[44] X. Wang, C.Y. Yan, A. Sumboja, J. Yan, P.S. Lee, Achieving high rate performance in layered hydroxide supercapacitor electrodes, Adv. Energy Mater. 4 (2014) 1301240.

[45] V. Pralong, A. Delahaye-Vidal, B. Beaudoin, J.B. Leriche, J.M. Tarascon, Electrochemical behavior of cobalt hydroxide used as additive in the nickel hydroxide electrode, J. Electrochem. Soc. 147 (2000) 1306–1313.
[46] R.C. Li, Z.X. Hu, X.F. Shao, P.P. Cheng, S.S. Li, W.D. Yu, W.R. Lin, D.S. Yuan, Large scale synthesis of NiCo layered double hydroxides for superior asymmetric electrochemical capacitor, Sci. Rep. 6 (2016) 18737.
[47] T. Yan, H.Y. Zhu, R.Y. Li, Z.J. Li, J.K. Liu, G.L. Wang, Z.Q. Gu, Microwave synthesis of nickel/cobalt double hydroxide ultrathin flowerclusters with three-dimensional structures for high-performance supercapacitors, Electrochim. Acta 111 (2013) 71–79.
[48] Y.F. Tang, Y.Y. Liu, S.X. Yu, W.C. Guo, S.C. Mu, H.C. Wang, Y.F. Zhao, L. Hou, Y.Q. Fan, F.M. Gao, Template-free hydrothermal synthesis of nickel cobalt hydroxide nanoflowers with high performance for asymmetric supercapacitor, Electrochim. Acta 161 (2015) 279–289.
[49] X.Q. Cai, X.P. Shen, L.B. Ma, Z.Y. Ji, C. Xu, A.H. Yuan, Solvothermal synthesis of NiCo-layered double hydroxide nanosheets decorated on RGO sheets for high performance supercapacitor, Chem. Eng. J. 268 (2015) 251–259.
[50] T. Li, G.H. Li, L.H. Li, L. Liu, Y. Xu, H.Y. Ding, T. Zhang, Large-scale self-assembly of 3D flower-like hierarchical Ni/Co-LDHs microspheres for high-performance flexible asymmetric supercapacitors, ACS Appl. Mater. Interfaces 8 (2016) 2562–2572.
[51] F.L. Lai, Y.P. Huang, Y.E. Miao, T.X. Liu, Controllable preparation of multi-dimensional hybrid materials of nickel-cobalt layered double hydroxide nanorods/nanosheets on electrospun carbon nanofibers for high-performance supercapacitors, Electrochim. Acta 174 (2015) 456–463.
[52] J. Pu, Y. Tong, S.B. Wang, E.H. Sheng, Z.H. Wang, Nickel-cobalt hydroxide nanosheets arrays on Ni foam for pseudocapacitor applications, J. Power Sources 250 (2014) 250–256.
[53] L. Ye, L.J. Zhao, H. Zhang, B. Zhang, H.Y. Wang, One-pot formation of ultra-thin Ni/Co hydroxides with a sheet-like structure for enhanced asymmetric supercapacitors, J. Mater. Chem. A 4 (2016) 9160–9168.
[54] H. Ashassi-Sorkhabi, P.L. Badakhshan, E. Asghari, Electrodeposition of three dimensional-porous Ni/$Ni(OH)_2$ hierarchical nano composite via etching the Ni/Zn/$Ni(OH)_2$ precursor as a high performance pseudocapacitor, Chem. Eng. J. 299 (2016) 282–291.
[55] Y.C. Zhu, W. Chu, N. Wang, T. Lin, W. Yang, J. Wen, X.S. Zhao, Self-assembled Ni/NiO/RGO heterostructures for high-performance supercapacitors, RSC Adv. 5 (2015) 77958–77964.
[56] X.T. Zheng, Y.L. Ye, Q. Yang, B.Y. Geng, X.J. Zhang, Ultrafine nickel-copper carbonate hydroxide hierarchical nanowire networks for high-performance supercapacitor electrodes, Chem. Eng. J. 290 (2016) 353–360.
[57] Y. Zhao, X. Zhang, J. He, L. Zhang, M. Xia, F. Gao, Morphology controlled synthesis of nickel cobalt oxide for supercapacitor application with enhanced cycling stability, Electrochim. Acta 174 (2015) 51–56.
[58] X.X. Liu, A. Zhou, T. Pan, Y.B. Dou, M.F. Shao, J.B. Han, M. Wei, Ultrahigh-rate-capability of a layered double hydroxide supercapacitor based on a self-generated electrolyte reservoir, J. Mater. Chem. A 4 (2016) 8421–8427.
[59] Y.Q. Jiang, L.Y. Chen, H.Q. Zhang, Q. Zhang, W.F. Chen, J.K. Zhu, D.M. Song, Two-dimensional Co_3O_4 thin sheets assembled by 3D interconnected nanoflake array framework structures with enhanced supercapacitor performance derived from coordination complexes, Chem. Eng. J. 292 (2016) 1–12.
[60] H. Ma, J. He, D.B. Xiong, J. Wu, Q. Li, V. Dravid, Y. Zhao, Nickel cobalt hydroxide @reduced graphene oxide hybrid nanolayers for high performance asymmetric supercapacitors with remarkable cycling stability, ACS Appl. Mater. Interfaces 8 (2016) 1992–2000.
[61] Y. Zhao, H. Ma, S. Huang, X. Zhang, M. Xia, Y. Tang, Z.F. Ma, Monolayer nickel cobalt hydroxyl carbonate for high performance all-solid-state asymmetric supercapacitors, ACS Appl. Mater. Interfaces 8 (2016) 22997–23005.
[62] R. Zhang, H. An, Z. Li, M. Shao, J. Han, M. Wei, Mesoporous graphene-layered double hydroxides free-standing films for enhanced flexible supercapacitors, Chem. Eng. J. 289 (2016) 85–92.
[63] B. Guan, Y. Li, B. Yin, K. Liu, D. Wang, H. Zhang, C. Cheng, Synthesis of hierarchical NiS microflowers for high performance asymmetric supercapacitor, Chem. Eng. J. 308 (2017) 1165–1173.